RSC Advances

Template fabricated plasmonic nanoholes on analyte-sensitive substrates for real-time vapor sensing

Journal:	*RSC Advances*
Manuscript ID:	RA-ART-02-2014-001797
Article Type:	Paper
Date Submitted by the Author:	14-Jan-2014
Complete List of Authors:	Lindquist, Nathan; Bethel University, Physics Turner, Mark; Bethel University, Physics Heppner, Benjamin; Bethel University, Physics

Template fabricated plasmonic nanoholes on analyte-sensitive substrates for real-time vapor sensing

Nathan C. Lindquist,[*,x] Mark Turner,[†,x] and Benjamin Heppner[†]

Physics Department, Bethel University, 3900 Bethel Drive, St Paul, MN 55112
[*] *email:* n-lindquist@bethel.edu
[*] *web:* https://sites.google.com/a/bethel.edu/ncl48757-nanolab/
[†] undergraduate students
[x] These authors contributed equally

Abstract: Sensing with nanostructured plasmonic devices has become an important research field due to their proven ability to be extremely sensitive, compact, multiplexed, and compatible with low-cost fabrication techniques. In this paper, we employ a modified template stripping method to produce plasmonic nanohole arrays on analyte-sensitive substrates for real-time vapor sensing. The device operates by exploiting simultaneous plasmonic resonances within the substrate as well as within the vapor being tested. Because the substrate is in contact with vapor due to the open-hole geometry, red-shifts (air-side resonances) and blue-shifts (substrate-side resonances) are seen at the same time during exposure to <10 ppm ethanol vapor in nitrogen. We also show negative control experiments with similar concentrations of m-xylene, as well as multiplex sensing potential with chemically patterned substrates. Our devices could operate as low-cost gas sensors for environmental monitoring, security, or food safety.

Keywords: plasmonics, gas sensing, template stripping, nanoholes, electronic nose, optical sensors, plasmonic sensors.

Introduction

The sensitive detection of gas phase analytes poses many significant challenges and opportunities from food safety and environmental monitoring to security and biomarker detection.[1, 2, 3] Of the available vapor sensing technologies, optical sensors allow probing test chambers remotely and analyzing refractive indices, molecular vibration and absorption spectra, and vapor concentrations to a high degree of accuracy and specificity.[4] However, reducing the size of the sensor typically relies on resonant devices in order to strengthen the interaction while providing a more compact form. In this regard, plasmonic optical biosensors[5] have become an important area of research because they are extremely sensitive to surface changes within subwavelength dimensions and show significant potential for on-chip integration, low cost processing, and massive parallelization. Furthermore, surface plasmons excited on the sensor surface can lead to surface enhanced effects such as surface enhanced Raman spectroscopy (SERS) for chemical identification.[6] Surface plasmons are wave oscillations of conduction electrons at the surface of a metal film. For visible frequencies, gold and silver substrates are typically used. If the metal contains nano-patterns, exquisite control of optical fields in sub-wavelength regions over the surface can be achieved.[7] Because plasmons are bound to the surface, the electric field only penetrates a small distance into the surrounding dielectric environment, probing it with high sensitivity. Additionally, the

electric field can be confined and enhanced by orders of magnitude compared to the incident field, leading to SERS, notably, but also super-focusing and squeezing of light.[8, 9]

Because of these unique attributes, plasmonic devices have found a wide range of cutting-edge applications, particularly in biosensing.[10] Indeed, the discovery of plasmon-enhanced optical transmission through an array of nano-structured holes[11] has led to the development of a new generation of optical biosensors.[12, 13, 14, 15, 16, 17, 18] These nanohole array sensors have been used in several configurations, such as in multichannel assays, sub-micron resolution imaging, and on-chip integration with microfluidics. While nanohole biosensors have been typically used in a liquid environment, plasmonic sensing of gas-phase analytes is also an important area of research and development.[19, 20, 21, 22, 23, 24] For example, plasmonic nanoparticles have been used to detect the refractive indices of various inert gasses[25] or for chemical identification via SERS.[2, 3]

It is also important to develop a sensor with some specificity. For example, self-assembled monolayers have been used to enhance the selectivity of nanoparticle-based gas-phase sensors.[26] Likewise, in liquid phase detection with plasmonic nanoholes, the surface is typically modified with a self-assembled monolayer of acceptor molecules.[27] Due to the unique open-hole geometry, nanohole-based sensors are also suitable for flow-through detection[28, 29] or in-pore sensing. In the case of a solid support, it is also therefore possible to involve the substrate itself in the detection process.

In this paper, we describe real-time gas sensing with plasmonic nanohole arrays on analyte-sensitive substrates produced via a template stripping method.[27] By modifying the template stripping technique, we are able to chemically pattern the substrate. Our demonstration of gas detection with plasmonic nanoholes shows response to less than 10 ppm ethanol vapor in nitrogen and uses real-time, high-resolution plasmon resonance tracking. Another advantage of our open-hole geometry is the fact that, since plasmons are sensitive only to surface changes, the analyte vapor only need interact with an extremely thin region of the analyte-sensitive substrate. Full three-dimensional computer simulations are used to verify our conclusions. We demonstrate simple multiplex sensing and imaging capability with a back-side patterning technique[30] that does not rely on more complicated electrochemical methods.[24] Finally, the device operates by exploiting simultaneous plasmonic resonances within the substrate as well as within the air or vapor being tested. This work presents results including: (1) Monitoring simultaneous plasmonic red-shifts and blue-shifts from both sides of the nanohole film; (2) Modifying the template stripping process to allow patterning the substrate before final assembly; (3) Using plasmonic nanoholes for gas sensing, of which the authors believe only ref. [24] has reported previously; and (4) The potential low-cost, high-quality fabrication benefits of template stripped surfaces that have not yet been used for vapor sensing.

Experimental

Figure 1 shows a schematic of our nanohole sensing platform and device fabrication. In order to create surface plasmons for sensing via the extraordinary optical transmission effect,[11] a high-quality nanohole array must first be fabricated, preferably over a large area. One such method of fabrication is by metal deposition onto a silicon template.[31,

32] This process involves fabricating a silicon master template, depositing a thin metal film, and then stripping the film from the template with an adhesive backing layer. The resultant surfaces are very smooth, and dozens of identical arrays can be created by reusing same template. While many other fabrication methods are available,[33] template stripping is ideal in our current case by offering the ability to chemically pattern the nanohole array substrate itself before stripping from the template. In this manner, we are able to fabricate multiplex, large area sensing chips.

The first step in fabrication is cleaning a commercially available silicon template (LightSmyth Technologies). We used a standard chromium etchant (Sigma-Aldrich) to remove leftover silver from previous depositions and a H_2O_2:H_2S0_4 (1:1) solution to treat the silicon surface and remove any contaminants. The template was then placed into a thermal evaporation chamber (Oxford Vacuum Science) and pumped to a pressure of $5*10^{-6}$ Torr. Silver was deposited at an average rate of 30 nm/min until a film of 50 nm accumulated on the template. After deposition, the template was removed and appeared as in figure 1b. A UV-curable adhesive (Norland 61) backing layer was then applied to a small area of the silver-coated template and a glass microscope slide was placed on top. The adhesive was cured and then stripped from the silicon template. Due to silver's poor adhesion to the silicon, the nanohole array was removed without damaging the template. The template was then be reused. An example of a stripped silver nanohole array on a glass template fabricated in this manor can be seen in figure 1f.

The experimental setup of figure 2 was designed to create a controlled sensing environment. This was done with a fluid pumping system that allows for precise control of gas flow rate and gas vapor concentration. A nitrogen gas mass flow controller (Cole Parmer) sets the flow rate for the entire system, typically between 200-400 mL/min. Next two three-way valves controlled the flow direction of the gas. Nitrogen can either flow directly into the sample chamber or through the mixing channel. In the mixing channel, nitrogen flows through a heated aluminum chamber where organic test compounds can be metered via a syringe pump (Cole Parmer) to evaporate and mix into the nitrogen flow. Since the mass flow rates of both the nitrogen and the organic liquids are precisely controlled, the vapor concentration can be determined and programmed. The gas then flows into a sample chamber and over the nanohole array after which it is vented.

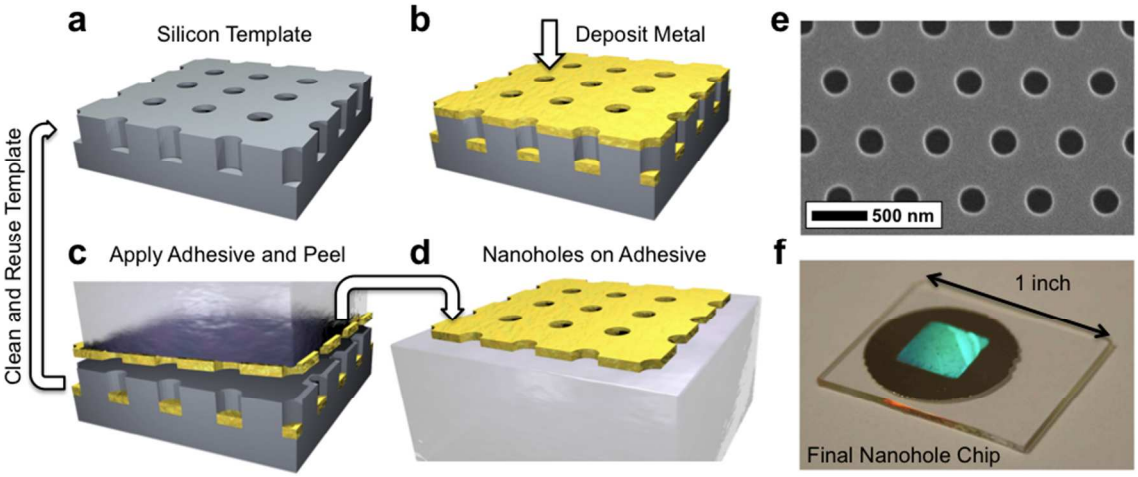

Figure 1: Nanohole device processing schematic. (a) A silicon template with 200 nm deep holes is purchased commercially and cleaned. (b) A thin silver layer is deposited onto the template, creating a continuous silver film with patterned nanoholes. (c) Due to the poor adhesion to the template, an adhesive backing layer is used to (d) peel off the patterned film. The template is then cleaned and reused. (e) Scanning electron micrograph (SEM) of the template. Image courtesy LightSmyth technologies, Inc. Used with permission. (f) Photograph of a representative nanohole chip. The adhesive layer bonds the chip to a rigid glass slide.

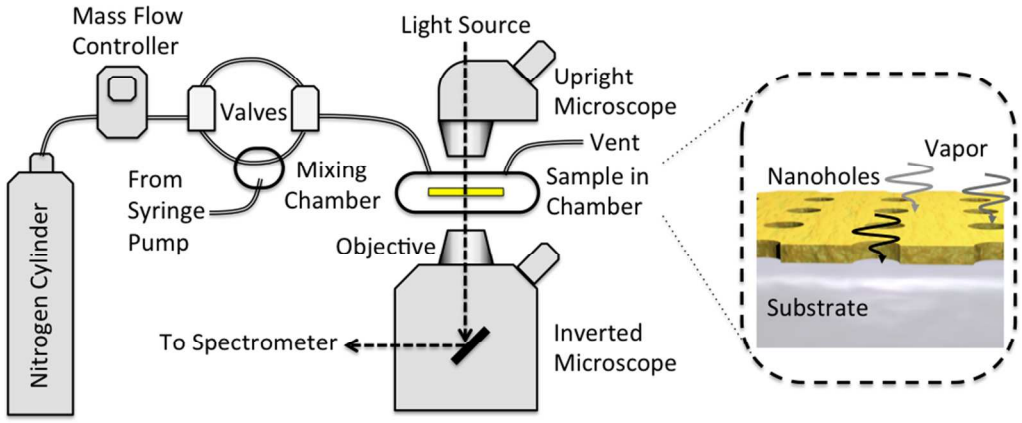

Figure 2: Vapor delivery and microscope setup. Purified nitrogen is mixed with vaporized organic compounds in a heated mixing chamber. By setting the delivery rate of the liquid into the heated vaporization chamber, the vapor concentration could be determined and delivered to the sensor chip in a controlled environmental chamber. A dual upright / inverted microscope system illuminates and passes transmitted light to a spectrometer for analysis. As the vapor mixtures pass over the nanoholes of the sensor chip, the open pores permit interaction with the substrate material.

The nanohole array sits between two microscopes (Nikon). Here, white light is collimated and then aligned over the array by the upright microscope. The transmitted light then travels through the inverted microscope and is sent to the imaging spectrometer (Horiba MicroHR) with a cooled EMCCD (PCO Sensicam EM). In the spectrometer, either a high (600 lines/mm) or a low resolution (100 lines/mm) grating was used to analyze the transmission spectrum. The spectrometer, camera, and gas system are all run with custom LabVIEW programs.

Tests begin by setting the nitrogen flow rate, vapor test concentrations, spectrometer exposure time, and saving a white light and dark spectrum in LabVIEW. The white light (directly through the glass slide without a silver layer) and dark spectra (shutter closed) are used to create a normalized spectrum of the transmitted light. Spectral data is then saved for several minutes with pure nitrogen running so a baseline measurement at 0 ppm can be made. Next, flow is switched to the mixing channel while the fluid pump is kept off. This step flushes any contaminants from the mixing channel before any ethanol or m-xylene fluid is added to the heated vaporization chamber. Ethanol or other organic fluids are then pumped into the mixing chamber at a desired flow rate to achieve specific concentrations in the nitrogen. As this change occurs in the gas, LabVIEW continues to save each transmission spectrum in real-time (roughly one per second) and tracks the position of a local minimum with dynamic least-squares curve fitting. After a shift in the

spectrum is observed, the fluid pump can be turned off and flow redirected to the clean channel.

Results and Discussion

Experimental runs were done with both the high-resolution and low-resolution spectrometer gratings to determine the sensitivity of our nanohole arrays. In addition to this, negative control testing was performed with m-xylene. The low-resolution spectrum (figure 3a) depicts several dips and peaks created by the plasmon-enhanced transmission process. For a hexagonal array of nanoholes, the plasmon resonance wavelengths $\lambda_{plasmon}$ are estimated via a grating coupling mechanism[34]

$$\lambda_{plasmon} = a\left[\frac{4}{3}(i^2 + ij + j^2)\right]^{-1/2}\sqrt{\frac{\varepsilon_m\varepsilon_d}{\varepsilon_m + \varepsilon_d}}$$

Where a is the period of the array, i and j represent the Bragg resonance orders, and ε_m and ε_d are the dielectric constants of the metal and the dielectric, respectively. Here, ε_d can represent either the air-side (ε_d = 1.00) or the substrate-side ($\varepsilon_d \approx 2.43$) resonances. While not accounting for the specific hole shape, film thickness and other parameters, this equation can be used to identify the grating-coupled plasmon resonances apparent in the transmission spectrum. It also predicts that a slight shift in either the air or substrate refractive index will cause a shift in the resonance wavelengths. In our devices, the period of the nanoholes was 700 nm. The dielectric constant of the adhesive substrate was taken from the manufacturer datasheet (Norland 61) and the dielectric constant of the silver was a Drude model fit ($\varepsilon_m \approx$ -13 at around 600 nm) to experimental optical constants.[35] In our data shown in figure 3a, the peaks (dips) at 610 nm (600nm) and 630 nm (620nm) appear to correspond to the *(i,j)=(1,1)* substrate-side and *(i,j)=(1,0)* air-side plasmon resonances, respectively. The peak near 570 nm corresponds to the *(i,j)=(2,0)* substrate-side plasmon. While the full transmission process is complex, surface plasmons play a role in the locations of both the transmission minima and maxima.[36, 37, 38, 39] In our experiments, while both the peaks and the dips shifted, we obtained better signals by tracking the transmission minima.

As the ethanol concentration in the system is adjusted, the resonance wavelengths will shift, also shown in figure 3a. In our case, with the Norland 61 adhesive substrate, both a red shift and blue shift are seen, and can be monitored in real time (figure 3b). The spectrum then returns to the baseline (0 ppm) resonance wavelengths as ethanol vapor is removed. The red shift occurs due to the air-side refractive index increasing with ethanol in the system, due to vapor on the silver surface.[21] The blue shift occurs due to the ethanol vapor interacting with the adhesive substrate, causing a reduction in its effective refractive index (the refractive index of ethanol is ~1.36 whereas the refractive index of the adhesive is ~1.56). The exact mechanism of this interaction is under further investigation, but perhaps it is due to the adhesive absorbing ethanol and expanding or to the ethanol preferentially accumulating at the silver-adhesive interface in or under the nanoholes. In any case, similar to other plasmonic thin-film gas sensors,[22] the analyte-sensitive layer we used has an affinity for ethanol vapor since negative control experiments with less polar m-xylene caused no shift in the substrate-side resonance wavelength (figure 3b).

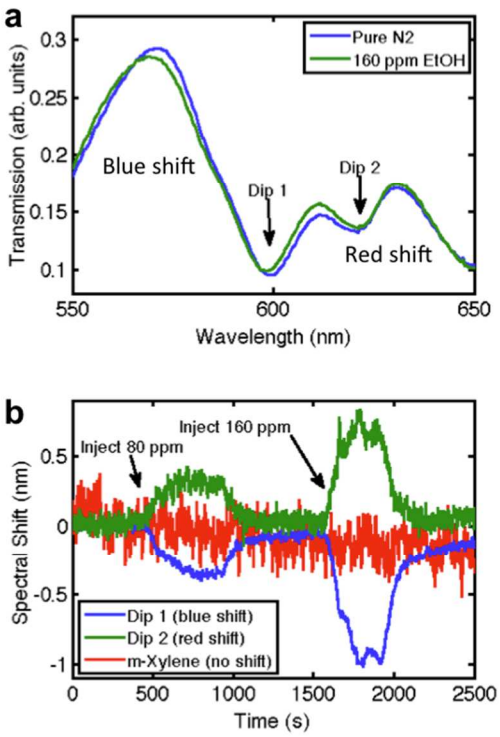

Figure 3: Experimental transmission spectra and real-time vapor sensing. (a) Normalized transmission spectrum of a 700 nm hexagonal nanohole array through a 50 nm thick silver film. The transmission peaks and dips correspond to plasmon-enhanced resonances. Due to a grating coupling mechanism, the peak (dip) near 610 nm (600 nm) corresponds to a substrate-side resonance while the peak (dip) near 630 nm (620 nm) corresponds to an air-side resonance. Upon exposure to 160 ppm ethanol vapor, "Dip 1" near 600 nm blue shifts by about 1.0 nm whereas "Dip 2" near 620 nm red shifts by about 0.7 nm. The peak near 570 nm also blue shifts, corresponding to a higher-order substrate-side resonance. (b) Tracking the position of the two resonance dips in real-time shows the sensor response to 80 ppm and 160 ppm ethanol vapor. The red shift on the air side is mainly due to increasing the bulk refractive index above the nanohole array whereas the blue shift is due to interaction of the ethanol vapor with the substrate, lowering its effective refractive index. A negative control experiment was run with 100 ppm of m-xylene vapor (also shown).

The high resolution scans (figure 4) produced similar results but with a higher sensitivity. Experiments with concentrations as low 10ppm were conducted. Our mixing chamber and syringe pump setup didn't allow concentrations lower than this. As can be seen in figures 4b and 4c, slight pulsing in the resonance wavelength occurs at these low concentrations. As the syringe pump was working near its lower limit, the mechanical pumping action could cause this behavior.

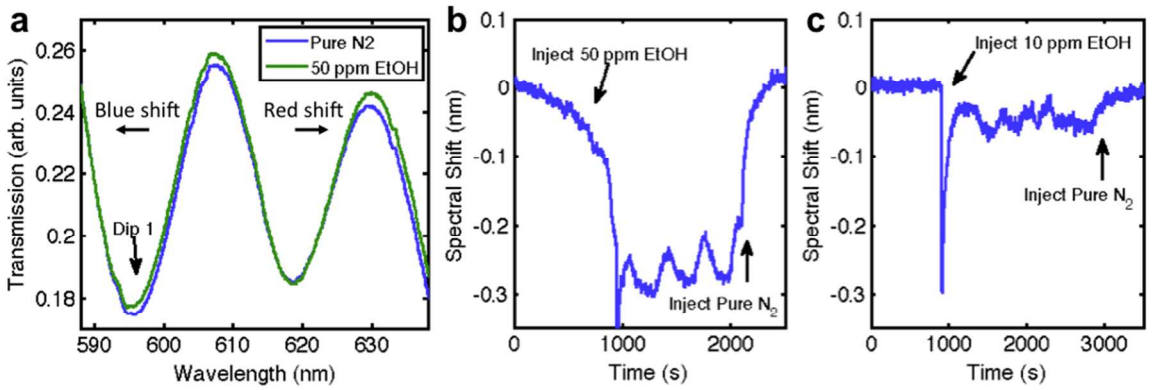

Figure 4: High-resolution transmission spectra and real-time sensing. (a) Using a higher-resolution spectrometer grating, higher sensitivity is obtained for both (b) 50 ppm ethanol vapor and (c) 10 ppm ethanol vapor. In this setup, the base noise level is nearing a ~1 ppm detection limit. The pulsing likely comes from the syringe pump operating at near its lower limit.

Finite element computer simulations (COMSOL) were created to view the plasmon resonance field distributions, the transmission spectra, and how shifts in air-side and substrate-side refractive indices would affect the resonance wavelengths. The simulations used periodic boundary conditions, a 50 nm thick silver film modeled with a Drude dispersion curve, and a 700 nm period hexagonal array with 200 nm diameter holes. Figure 5a displays the transmission spectrum and, coinciding well with our experimental data, there are transmission peaks at roughly 550 nm and 660 nm, and a series of dips at 600 nm and 620 nm. The peak near 610 nm corresponds to an *(i,j) = (1,1)* adhesive-side peak (as in figure 3a) but is also close to a *(1,0)* air-side Wood's anomaly.[40] The refractive indexes were then manually altered from 1.00 to 1.01, for the air side, and 1.56 to 1.55 for the substrate side. What resulted was a blue shift in the substrate side resonances and a red shift in the air side resonances, as expected. Because the experimental data is acting in a similar way for the corresponding peaks and dips, this simulated data is a good indicator that the adhesive is interacting with the ethanol is some manner that decreases refractive index while the air increases in refractive index. Figure 5b and 5c simulate the electric fields created by the surface plasmons. Plasmons are being created on both sides of the nanohole array (depending on the wavelength) and extend only a short distance into the surrounding environment.

Finally, we ran tests with the nanohole arrays that involved sensing over different areas of the chip simultaneously with a patterned substrate. This involved patterning different areas of the nanohole array with different gas-sensitive materials prior to template stripping. Beyond this simple scheme described here, having multiple sections that are sensitive to multiple individual unique gasses would allow our nanohole arrays to detect multiple gasses at the same time with very high accuracy. Figure 6 shows initial experiments with such multiplex sensing capability by using the UV adhesive, sensitive to the ethanol, surrounded by a cyanoacrylate glue (Loctite), insensitive to the ethanol. Each area had a unique transmission spectrum due to the slightly different refractive indices of the substrate material. Both areas were monitored in real-time simultaneously with our LabVIEW program. When ethanol was introduced to the system, the substrate-side resonance in the UV adhesive region blue shifted, as before. However, the superglue resonance wavelength slightly red shifted. Future testing is under way with other

materials to determine chemical sensitivity to various vapors and to show large-scale multiplex sensing capabilities with this straightforward substrate patterning scheme.

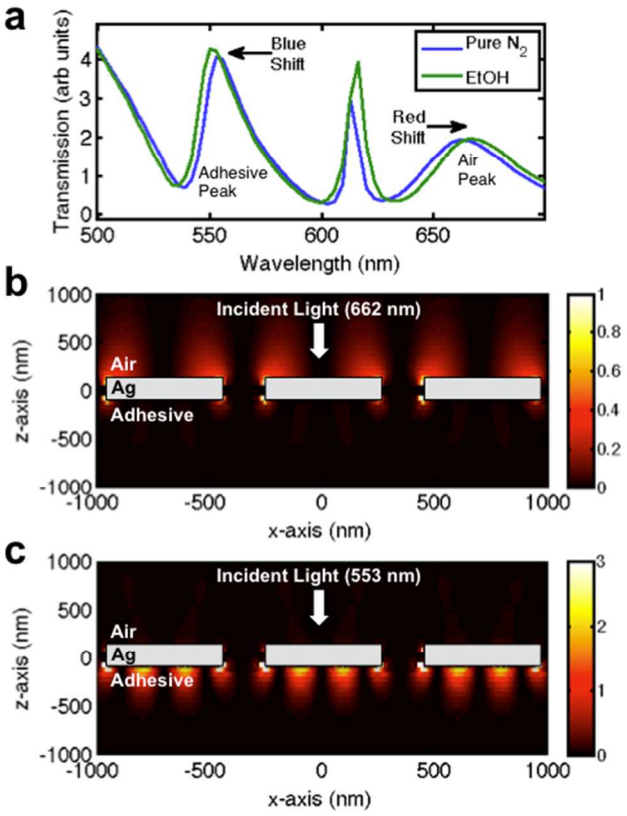

Figure 5: Simulated transmission data. (a) Simulated nanohole transmission curves for a device equivalent to that in figure 3a, showing good agreement. The adhesive-side and air-side peaks are labeled. The introduction of ethanol vapor was modeled by increasing the refractive index of the air from 1.00 to 1.01 and decreasing the refractive index of the substrate from 1.56 to 1.55. The peaks shifted accordingly. (b) Simulated field maps (time averaged z-component of the electric field) of the *(1,0)* air-side resonance peak at 662 nm and (c) the *(2,0)* substrate-side resonance peak at 553 nm. The evanescent plasmon fields probe only a short distance into the surrounding environment, showing sensitivity to either the air side (b) or the substrate side (c).

Conclusions

We have demonstrated that gas-specific testing is possible with silver nanohole arrays supported by chemically sensitive substrate materials. Indeed, with stable light sources and high-resolution spectroscopy, plasmonic wavelength shifts less than 0.01 nm are detectable,[25] meaning that a reasonable sensitivity limit in our devices could reach <1 ppm. Fabricating nanohole array chips with multiple materials is straightforward with our backside template stripping technique, allowing multiple, chemically unique sensors on a single chip. Such a sensor can be easily scaled down in size, and chemically active substrates could be patterned via photolithography. These devices could be applied in multiple fields due to their low cost, small size, multiplex capability, and high sensitivity.

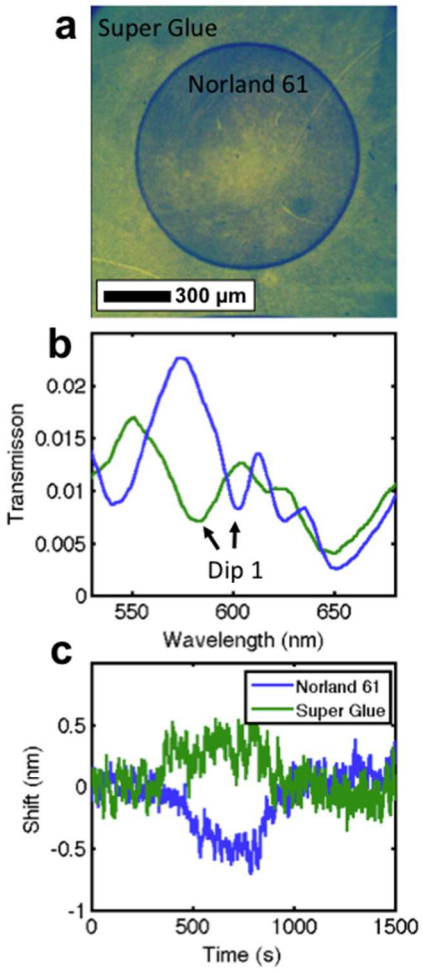

Figure 6: Multiplex sensing capability. (a) To demonstrate multiplexing capability, another device was fabricated with a central dot of the UV curable Norland 61 adhesive surrounded by a region of cyanoacrylate superglue. (b) The two transmission spectra are offset due to the two different refractive indices but the spectra have a similar overall shape. (c) Upon exposure to 200 ppm ethanol vapor, the central Norland 61 area responded in the same manner shown previously (with both blue shifts and red shifts) while the Super Glue region showed only a slight red shift of both the air-side and substrate-side resonances. These results show marked differences in the side-by-side regions, demonstrating multiplex potential by simply patterning the substrate prior to template stripping.

Acknowledgements

The authors thank Phil Minell and James Myrick (US Engi*new*ing) for collaborative discussion and support. Parts of this research were also supported by the Minnesota Space Grant Consortium (MnSGC), part of the NASA Funded National Space Grant College and Fellowship Program.

References

1. Whittle, C. L., Fakharzadeh, S., Eades, J., and Preti, G., "Human breath odors and their use in diagnosis," Annals of the New York Academy of Sciences 1098, 252--266 (2007).

2. Biggs, K. B., Camden, J. P., Anker, J. N., and Duyne, R. P. V., "Surface-Enhanced Raman Spectroscopy of Benzenethiol Adsorbed from the Gas Phase onto Silver Film over Nanosphere Surfaces: Determination of the Sticking Probability and Detection Limit Time†," The Journal of Physical Chemistry A 113, 4581--4586 (2009).
3. Stuart, D. A., Biggs, K. B., and Duyne, R. P. V., "Surface-enhanced Raman spectroscopy of half-mustard agent," Analyst 131, 568--572 (2006).
4. Hodgkinson, J. and Tatam, R. P., "Optical gas sensing: a review," Measurement Science and Technology 24, 012004 (2013).
5. Stewart, M. E., Anderton, C. R., Thompson, L. B., Maria, J., Gray, S. K., Rogers, J. A., and Nuzzo, R. G., "Nanostructured plasmonic sensors," Chemical Reviews 108, 494--521 (2008).
6. Haynes, C. L., McFarland, A. D., and Van Duyne, R. P., "Surface Enhanced Raman Spectroscopy," Analytical Chemistry 77, 338A (2005).
7. Barnes, W. L., Dereux, A., and Ebbesen, T. W., "Surface plasmon subwavelength optics," Nature 424, 824 (2003).
8. Gramotnev, D. K. and Bozhevolnyi, S. I., "Plasmonics beyond the diffraction limit," Nature Photonics 4, 83--91 (2010).
9. Lindquist, N. C., Jose, J., Cherukulappurath, S., Chen, X., Johnson, T. W., and Oh, S.-H., "Tip-Based Plasmonics: Squeezing Light with Metallic Nanoprobes," Laser and Photonics Review 7, 453 (2013).
10. Brolo, A. G., "Plasmonics for future biosensors," Nature Photonics 6, 709--713 (2012).
11. Ebbesen, T. W., Lezec, H. J., Ghaemi, H. F., Thio, T., and Wolff, P. A., "Extraordinary optical transmission through sub-wavelength hole arrays," Nature 391, 667 (1998).
12. Gordon, R., Sinton, D., Kavanagh, K. L., and Brolo, A. G., "A new generation of sensors based on extraordinary optical transmission," Accounts of Chemical Research 41, 1049 (2008).
13. De Leebeeck, A., Kumar, L. K. S., de Lange, V., Sinton, D., Gordon, R., Brolo, A. G., and others, "On-chip surface-based detection with nanohole arrays," Anal. Chem 79, 4094--4100 (2007).
14. Tetz, K. A., Pang, L., and Fainman, Y., "High-resolution surface plasmon resonance sensor based on linewidth-optimized nanohole array transmittance," Optics Letters 31, 1528 (2006).
15. Brolo, A. G., Gordon, R., Leathem, B., and Kavanaghs, K. L., "Surface plasmon sensor based on the enhanced light transmission through arrays of nanoholes in gold films," Langmuir 20, 4813--4815 (2004).
16. Im, H., Lesuffleur, A., Lindquist, N. C., and Oh, S. H., "Plasmonic Nanoholes in a Multichannel Microarray Format for Parallel Kinetic Assays and Differential Sensing.," Analytical Chemistry 81, 2854 (2009).
17. Lindquist, N. C., Lesuffleur, A., Im, H., and Oh, S. H., "Sub-micron resolution surface plasmon resonance imaging enabled by nanohole arrays with surrounding Bragg mirrors for enhanced sensitivity and isolation," Lab on a Chip 9, 382--387 (2009).
18. Lee, S. H., Lindquist, N. C., Wittenberg, N. J., Jordan, L. R., and Oh, S.-H., "Real-time full-spectral imaging and affinity measurements from 50 microfluidic channels using nanohole surface plasmon resonance," Lab on a Chip 12, 3882--3890 (2012).
19. Liedberg, B., Nylander, C., and Lundstrom, I., "Surface plasmon resonance for gas detection and biosensing," Sensors and Actuators 4, 299 (1983).
20. Nylander, C., Liedberg, B., and Lind, T., "Gas detection by means of surface plasmon resonance," Sensors and Actuators 3, 79--88 (1983).
21. Vukusic, P., Bryan-Brown, G., and Sambles, J., "Surface plasmon resonance on gratings as a novel means for gas sensing," Sensors and Actuators B: Chemical 8, 155--160 (1992).
22. Miwa, S. and Arakawa, T., "Selective gas detection by means of surface plasmon resonance sensors," Thin Solid Films 281, 466--468 (1996).
23. Notcovich, A. G., Zhuk, V., and Lipson, S., "Surface plasmon resonance phase imaging," Applied Physics Letters 76, 1665--1667 (2000).

24. Wright, J. B., Cicotte, K. N., Subramania, G., Dirk, S. M., and Brener, I., "Chemoselective gas sensors based on plasmonic nanohole arrays," Optical Materials Express 2, 1655--1662 (2012).
25. Bingham, J. M., Anker, J. N., Kreno, L. E., and Van Duyne, R. P., "Gas sensing with high-resolution localized surface plasmon resonance spectroscopy," Journal of the American Chemical Society 132, 17358--17359 (2010).
26. Chen, Y.-Q. and Lu, C.-J., "Surface modification on silver nanoparticles for enhancing vapor selectivity of localized surface plasmon resonance sensors," Sensors and Actuators B: Chemical 135, 492--498 (2009).
27. Im, H., Lee, S. H., Wittenberg, N. J., Johnson, T. W., Lindquist, N. C., Nagpal, P., Norris, D. J., and Oh, S. H., "Template-Stripped Smooth Ag Nanohole Arrays with Silica Shells for Surface Plasmon Resonance Biosensing," ACS Nano 5, 6244 (2011).
28. Eftekhari, F., Escobedo, C., Ferreira, J., Duan, X., Girotto, E. M., Brolo, A. G., Gordon, R., and Sinton, D., "Nanoholes as nanochannels: flow-through plasmonic sensing," Analytical Chemistry 81, 4308--4311 (2009).
29. Escobedo, C., Brolo, A. G., Gordon, R., and Sinton, D., "Flow-through vs flow-over: analysis of transport and binding in nanohole array plasmonic biosensors," Analytical chemistry 82, 10015--10020 (2010).
30. Lindquist, N. C., Johnson, T. W., Jose, J., Otto, L. M., and Oh, S. H., "Ultrasmooth metallic films with buried nanostructures for backside reflection-mode plasmonic biosensing," Annalen der Physik 524, 687 (2012).
31. Nagpal, P., Lindquist, N. C., Oh, S. H., and Norris, D. J., "Ultrasmooth patterned metals for plasmonics and metamaterials," Science 325, 594 (2009).
32. Lindquist, N. C., Johnson, T. W., Norris, D. J., and Oh, S. H., "Monolithic Integration of Continuously Tunable Plasmonic Nanostructures," Nano Letters 11, 3526 (2011).
33. Lindquist, N. C., Nagpal, P., McPeak, K. M., Norris, D. J., and Oh, S.-H., "Engineering metallic nanostructures for plasmonics and nanophotonics," Reports on Progress in Physics 75, 036501 (2012).
34. Thio., T., Ghaemi, H. F., Lezec, H. J., Wolff, P. A., and Ebbesen, T. W., "Surface-plasmon-enhanced transmission through hole arrays in Cr films," Journal of the Optical Society of America B 16, 1743 (1999).
35. Johnson, P. B. and Christy, R. W., "Optical constants of the noble metals," Physical Review B 6, 4370 (1972).
36. Garcia de Abajo, F. J., "Light scattering by particle and hole arrays," Reviews of Modern Physics 79, 1267 (2007).
37. Liu, H. and Lalanne, P., "Microscopic theory of the extraordinary optical transmission," Nature 452, 728 (2008).
38. Genet, C., Van Exter, M. P., and Woerdman, J. P., "Fano-type interpretation of red shifts and red tails in hole array transmission spectra," Optics Communications 225, 331 (2003).
39. Sarrazin, M., Vigneron, J. P., and Vigoureux, J. M., "Role of Wood anomalies in optical properties of thin metallic films with a bidimensional array of subwavelength holes," Physical Review B 67, 85415 (2003).
40. Chang, S. H., Gray, S. K., and Schatz, G. C., "Surface plasmon generation and light transmission by isolated nanoholes and arrays of nanoholes in thin metal films," Optics Express 13, 3150--3165 (2005).